Migration of point defects at charged Cu, Ag, and Au (100) surfaces

J. E. Müller and H. Ibach
Institut für Schicht- und Grenzflächen, Forschungszentrum Jülich, D-52425 Jülich, Germany
(Received 7 December 2005; revised manuscript received 10 May 2006; published 15 August 2006)

We report *ab initio* values for the electrical dipole moment and for the formation and activation energies of adatoms and vacancies migrating on Cu, Ag, and Au (100) surfaces, and we discuss the effect of the electrical dipole energy of these point defects on the rate of mass transport along charged metal-electrolyte interfaces. We find that adatoms and vacancies exhibit positive surface dipole moments, which for positive electrode potentials tend to reduce the formation and activation energies and increase the mobility of the point defects. We also consider atom migration by an exchange process involving the intermediate formation of dimers, and find that the surface dipole moment of the Cu and Ag dimers is negative, which means that they tend to become more mobile for negative potentials. However, because of their large activation energies, we conclude that the exchange process is not likely to provide an energetically favorable mechanism for migration in these systems. The Au dimer has a small positive dipole moment, which implies that the exchange process may contribute to surface transport but only in neutral surfaces.

DOI: 10.1103/PhysRevB.74.085408 PACS number(s): 68.35.Md, 68.43.Bc, 68.43.Jk

I. INTRODUCTION

Point defects (adatoms and vacancies) are the main carriers in mass transport processes on metal surfaces and play an important role in surface phenomena such as epitaxial growth, coarsening, and thermal annealing, where the rate of mass transport is determined by the formation and activation energies of the point defects. These energies play also an important role in the structuring of charged solid-electrolyte interfaces, including processes like electrochemical annealing,[1–7] and in equilibrium fluctuations of monoatomic steps.[8–10] Since the initial and final states of surface transport processes are both on the surface, the driving force of these processes is given by the temperature of the system and is not directly affected by the electrode potential. However, in a recent presentation, Giesen *et al.* showed that for solid electrodes held in an electrolyte at a constant potential, all defect formation and activation energies become renormalized by the electrostatic energy of the defect dipoles.[11] As a consequence of this energy renormalization, the mobility of the point defects become dependent of the electrode potential. Since in typical electrochemical systems the electrostatic dipole energy is of the same order of magnitude as the formation and activation energies of the point defects, this potential dependence is experimentally readily observable.[1–11] Therefore, in order to properly describe the mass transport along charged solid-electrolyte interfaces we not only need information about formation and activation energies of the surface defects leading to surface mass transport, but also a detailed knowledge of their electrical properties. In this paper we present *ab initio* results for the formation and activation energies for migration, as well as for the electrical dipole moments of adatoms and vacancies at the Cu, Ag and Au (100) surfaces, and we discuss the role played by the electrostatic dipole energy in the mass transport by point defects at charged metal-electrolyte interfaces as a function of the applied potential. We find the surface dipole moment of both adatoms and vacancies to be positive, i.e., such that their mobility increases as a function of positive potentials applied to the metal-electrolyte interface.

Feibelman showed that for the Al (100) surface, the dominant migration mechanism is provided by an exchange process involving an intermediate step characterized by the formation of dimers.[12] In order to assess the relevance of this mechanism for the systems studied in this work, we also calculate the energies and electrical dipoles of dimers on the Cu, Ag, and Au (100) surfaces. For the Cu and Ag surfaces the dipole moment of the dimers turned out to be negative. We also found the exchange process to be energetically unfavorable compared with that of adatom and vacancy migration. Therefore we conclude that the exchange process is not likely to provide an energetically favorable mechanism for mass transport in these systems. On the other hand, for the Au (100) surface the energy of the dimer is comparable with that of the adatom. However, since the dipole moment of the Au dimer is rather small the exchange process is likely to play a role in surface migration only for neutral surfaces. In spite of its limited practical relevance, the dimer calculation provided an interesting insight on the formation of point-defect dipoles, for it showed that the Smoluchowsky principle does not provide a safe guide to predicting the sign of surface dipoles.

Several *ab initio* calculations of formation and activation energies of point defects have been reported. As a part of a detailed study of surface transport Stumpf and Scheffler presented *ab initio* results of the formation and activation energies and electrical dipole moments of adatoms, vacancies and dimers at various Al surfaces,[13] Yu and Scheffler reported formation and activation energies of adatoms and dimers on Ag(100),[14] and Polatoglou *et al.* calculated vacancy formation energies at the (111) surfaces of Al, Cu, Ag, and Rh.[15] Boisvert *et al.* calculated adatom activation energies for the (100) and (111) surfaces of Ag, Au, and Ir surfaces,[16] for the Pt(100) surface,[17] as well as adatom and vacancy activation energies for the Cu(100) surface.[18] Using the Car-Parrinello method Lee *et al.* obtained the activation energies of adatoms and dimers at the Cu (100) surface.[19]

It is important to point out that the physical quantities which determine the process of island decay (including Oswald ripening) in neutral surfaces are the activation energy

for diffusion and the equilibrium concentration of the migrating species, which in turn depends on the formation energy of the point defect E_{pd} according to

$$\rho = \frac{1}{\Omega_s} e^{-E_{pd}/kT}, \tag{1}$$

where Ω_s is the area of one surface atom. The formation energy E_{pd} is defined as the energy required to bring the diffusing species from a kink in straight step to a terrace site. Desorption or adsorption of a kink atom is not only the decay process of minimal energy but it also leaves the structure of the step unchanged, and therefore determines the equilibrium concentration. For other side conditions E_{pd} in Eq. (1) should be replaced by the appropriate thermodynamic potential, as we discuss below. In the present work we followed the previous considerations and studied a process in which an island at the (100) surface decays by the creation or annihilation of any of the point defects mentioned above with simultaneous removal of an atom located at a kink in a straight step bounding the island. By making contact with the appropriate thermodynamics, our calculations of the formation energies go beyond the scope of the previously reported studies in describing the energetic of island decay.

For an island of mesoscopic dimensions the electric dipole moment of the island is not affected by the removal of one atom, so that the change in the surface dipole moment in the decay process is just given by the dipole moment of the point defect created or annihilated. However, in our calculations the islands have microscopic dimensions so that this conclusion is not necessarily true. Therefore, we found it necessary to perform separate, more accurate calculations, independent of the creation and/or annihilation process to evaluate the electrical dipole moment of the point defects. For these separate calculations we considered the migration of the point defect on the terrace of a smooth (100) surface.

The present calculations were performed using the cluster approach. A small fraction of the (100) surfaces of Cu, Ag, and Au was modeled using appropriate metal clusters and the top layer of the clusters was modified to simulate the different point defects. The results presented below were obtained using clusters containing about 50 metal atoms. We have also performed calculations with smaller clusters of about 25 and 38 atoms, which showed that cluster size effects amount to less than 8% in the adsorption energies for all cases studied. The step atoms as well as those surrounding the point defects were allowed to relax, but the rest of the atoms of the cluster were fixed to the known experimental values.[21–23] The calculations included full relativistic cores, as well as scalar relativistic corrections for the valence electrons. The one-electron problem for the valence electrons (including *d*-states) was solved by expanding the single-particle wave functions in a localized muffin-tin orbital basis,[20] and the exchange and correlation contributions were evaluated using the local density approximation (LDA). The LDA tends to overestimate the hollow-site adsorption energies for the late transition metals by about 10% compared with those calculated with the generalized gradient approximation (GGA). These considerations must be taken into account when comparing our numerical results with available experimental and theoretical data.

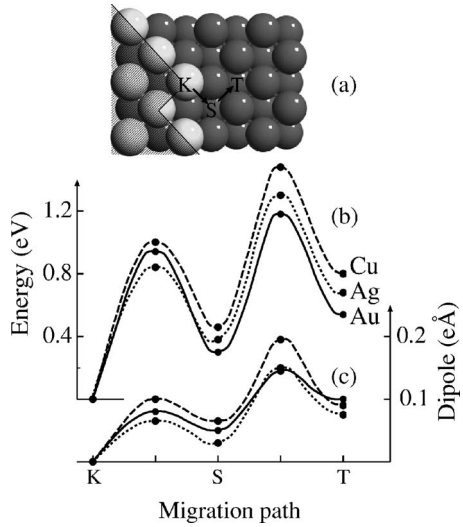

FIG. 1. (a) Cluster utilized to study the reaction path involved in the desorption of an atom from a kink in a step at the (100) surface. (b) Variation of the energy and (c) surface dipole moment of the adatom moving along the path $K \rightarrow S \rightarrow T$, indicated in inset (a), for the Au (full), Ag (dotted), and Cu (dashed) surfaces.

II. ADATOM MIGRATION

In this section we study the process by which an atom desorbs from a kink at a step and migrates as an adatom along a terrace of the Cu, Ag, and Au (100) surfaces. As mentioned in the introduction, the processes of adatom formation and of adatom migration along the terrace will be considered separately in two different calculations. To study the creation of the adatom we employ asymmetrical clusters and allow for large atomic displacements. For the migration of the adatom along the flat surface we use symmetrical clusters and consider adatom displacements which are much smaller (from one adsorption site to the next). The results of the second calculation are expected to be more reliable and will taken as reference values. The two sets of calculations were found to be consistent with each other within less than 5%.

Figure 1(a) shows the 49-atom cluster utilized to study the creation of the adatom. The bright shaded area represents a small fraction of an island bounded by a step with a kink. The dark nonshaded area represents a small fraction of the terrace of a (100) metal surface. The migration path marked on the figure was found to exhibit the smallest activation energy and to provide the most probable mechanism for island decay. It illustrates an atom desorbing from the kink-site *K* and moving along the step up to site *S* and further desorbing from the step into a terrace site *T*. An alternative reaction path in which the kink-atom directly desorbs into the terrace exhibits larger intermediate energies, for the transition state of an adatom bound to the step has about 0.15 eV less energy than the transition state of an adatom in the terrace.

Figures 1(b) and 1(c) show the variation of the energy and of the electric dipole moment along the migration path *K*

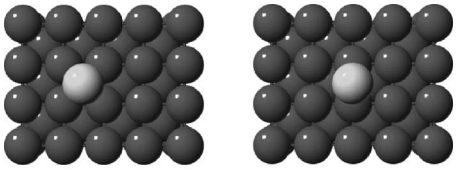

FIG. 2. 53-atom clusters utilized to represent an adatom adsorbed on a (100) surface, moving from (a) the ground state above a fourfold coordinated hollow site to (b) the transition state above a twofold coordinated bridge site.

$\rightarrow S \rightarrow T$, including intermediate positions. For each position in the surface plane we varied the height of the adatom and we calculated the local equilibrium geometry, the energy, and the surface dipole moment of the system. We observe that the adatom energy and dipole moment are larger in the twofold bridge sites than in the fourfold hollow sites, giving rise to an activation barrier for migration along the surface. The three systems studied in this work show qualitatively the same behavior as a function of migration distance, whereby for Cu the energies and dipole moments are somewhat larger. Notice that the first activation barrier at the surface step is smaller than that for migration along the surface, which means that adatom mediated decay is diffusion limited.

In order to evaluate the adatom formation energy E_a we assume that far away from the surface step the variation of the energy along the migration path repeats the oscillation found between S and T. Therefore, we take

$$E_a = E_a(T) - E_a(K), \tag{2}$$

where $E_a(K)$ and $E_a(T)$ are the energies of the adatom at the locations T and K displayed in Fig. 1(b).

In order to study the migration of an adatom along the terrace of the (100) metal surface we employed the 53-atom clusters shown in Fig. 2. The cluster of Fig. 2(a) simulates the adatom adsorbed at the ground state fourfold hollow site. The cluster of Fig. 2(b) represents the adatom at the twofold bridge adsorption site, which is the transition state for surface diffusion, i.e., the site determining the height of the potential barrier along the migration path. We calculated the potential energy of the system as a function of height z of the adatom above the surface for both cases, and from the potential energy function we deduced the equilibrium geometry $z=z_a$, and the activation energy ΔE_a as the adatom move from the ground state to the transition state, where the height of the adatom increases by Δz_a. We also calculated the corresponding change in the electric dipole moment $\Delta\mu_a$ and formation dipole moment μ_a. The reference cluster representing the smooth surface without the adatom, includes three atom layers, whereby the upper and lower layers are identical, such that the cluster is symmetrical in all three coordinates and has no electrical dipole moment. The formation dipole moment of the adatom μ_a is therefore given by the dipole moment of the cluster from Fig. 2(a) at the equilibrium geometry. As discussed in the introduction, there is a small discrepancy (of about 5%) between the energies calculated using the clusters of Figs. 1(a) and 2(a), due to the small size of the island used in the former calculation, whereby only the more accurate values will be reported in this work.

TABLE I. Calculated values for the formation energy E_a, activation energy ΔE_a, surface dipole moment μ_a, activation dipole moment $\Delta\mu_a$, adsorption height z_a, vibration frequency ω, and effective charge q_a^*, of an adatom adsorbed on the Cu, Ag, and Au (100) surfaces. The transition state energy $E_{a0}^+ = E_a + \Delta E_a$ and dipole $\mu_a^+ = \mu_a + \Delta\mu_a$ are discussed in Sec. V.

	Cu	Ag	Au
E_a	0.81 eV	0.68 eV	0.54 eV
ΔE_a	0.67 eV	0.62 eV	0.64 eV
E_{a0}^+	1.48 eV	1.30 eV	1.18 eV
μ_a	$0.092e$ Å	$0.076e$ Å	$0.095e$ Å
$\Delta\mu_a$	$0.103e$ Å	$0.072e$ Å	$0.049e$ Å
μ_a^+	$0.195e$ Å	$0.148e$ Å	$0.144e$ Å
z_a	1.51 Å	1.85 Å	1.81 Å
Δz_a	0.35 Å	0.38 Å	0.38 Å
ω_a	188 cm^{-1}	122 cm^{-1}	117 cm^{-1}
q_a^*	$0.20e$	$0.14e$	$0.03e$

The main results of the adatom calculation are summarized in Table I, where we also included the calculated vibration frequency ω_a, and the effective charge on the adatom, $q_a^* = (1/2) d\mu_a/dz$. We note that the Cu adatom exhibits larger charging as well as a more compact structure with larger binding energies and vibration frequencies, but results for the three metals are otherwise quite similar. Our results for the activation energies ΔE_a are in good agreement with previously reported LDA values: 0.75 eV (Ref. 18) and 0.69 eV (Ref. 19) for Cu(100), 0.50 eV for Ag(100) (Ref. 18) and 0.62 for Au(100) (Ref. 16). The GGA yields values that are smaller by 0.07 eV for Ag(100) (Ref. 14) and 0.20 eV for Cu(100) (Ref. 18), where we note the last discrepancy to be unexpectedly large. We cannot directly compare our formation energies E_a with published values, for previous authors systematically used different initial states for the creation process. Note, however, that both the creation of an adatom from a kink site and the hopping of an adatom through a bridge site involve the severance of two metal-metal bonds, so that we may reasonably expect $E_a \approx \Delta E_a$, as we found in our calculations.

The adsorption of the adatom induces a surface dipole moment with positive sign (such as to locally reduce the work function) for all three systems studied in this work. The physical origin of the positive adatom dipole moment can be visualized in Fig. 3 for the case of the Au(100) surface. Figure 3(b) shows the redistribution of charge induced by the adatom-surface bond in the symmetry [110] plane perpendicular to the surface, as given by the charge density difference,

$$\Delta\rho_a = \rho(\mathrm{Au}_{53}) - \rho(\mathrm{Au}_{52}) - \rho(\mathrm{Au}), \tag{3}$$

where Au_{53} is the cluster shown in Fig. 2(a), and Au_{52} the corresponding reference cluster without the adatom. We ob-

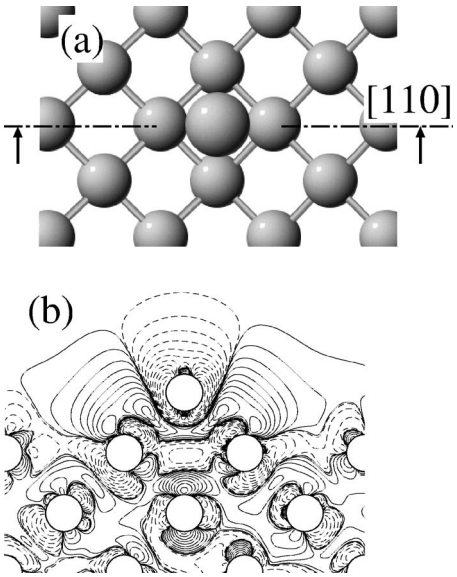

FIG. 3. (a) Schematic view of an adatom adsorbed on an Au(100) surface in the ground state geometry. (b) Change in the charge density induced in the [110] plane by the adsorption of the adatom. The continuous and dashed contour lines represent increase and decrease of charge, with densities given by $2n^3 \times 10^{-4}e$ Å^{-3}, for $n=-15,\ldots,15$.

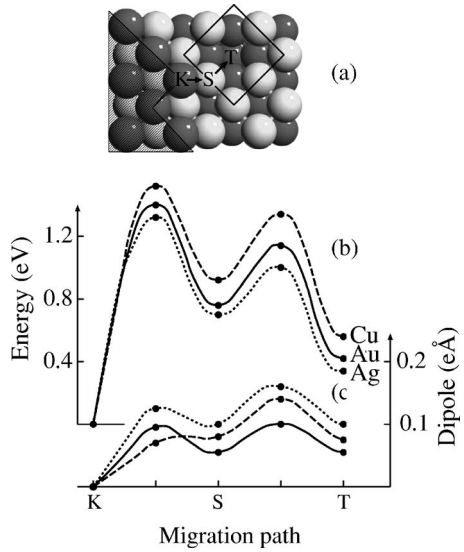

FIG. 4. (a) Cluster utilized to study the annihilation of a vacancy moving from the terrace to a kink in the (100) surface. The arrows indicate the movement of the atoms, which has the opposite direction than the movement of the vacancy. (b) Variation of the energy and (c) surface dipole moment of the vacancy moving along the path $T \leftarrow S \leftarrow K$, indicated in inset (a), for the Au (full), Ag (dotted), and Cu (dashed) surfaces.

serve that there is a decrease of the charge density on the volume of the adatom, and that the charge density of the surface is pushed away sidewards and away from the surface by the adatom. Using Mullikan populations,[24] the charge redistribution $\Delta\rho_a$ can be related to a change in the occupied cluster wave functions, a change which is realized by occupation of states that were unoccupied in the noninteracting systems. This means that the regions with large density of unoccupied states are the chemically active regions of the surface, and that the bonding of the adatom to the surface must lead to a charge transfer into these regions. Since each atom contributes roughly the same number of unoccupied states, the largest density of them is necessarily located towards the metal surface below the adatom, where the atomic density is larger. Therefore the surface bond produces a depletion of charge on the adatom and an increase of charge on the surface, and gives rise to the positive surface dipole moment.

The magnitude of the electric dipole moment depends on an electronic factor and a geometrical factor. The electronic factor is related to the strength of the atom-atom interaction of the species involved, and the geometrical factor to their atomic sizes. Since the electronic and geometric factors vary in opposite ways as a function of atomic number, we cannot predict a priori a clear trend in the Cu, Ag, Au series. The $3d$ states of Cu are much more unrestricted and reactive and lead to stronger bonds than the d functions of Ag and Au, which are required to be orthogonal to the core and therefore are much stiffer and less reactive. On the other hand, the larger atomic size of Ag and Au tends to bring about larger dipole moment values for these systems. The fact that Cu exhibits larger dipole moments and energies indicates that the electronic effect is the dominant one. Ag and Au have comparable dipole moment values because of the relativistic contraction of the Au core.

III. VACANCY MIGRATION

In this section we study a process by which a vacancy at the terrace of a (100) surface moves towards a kink in a step and is annihilated by the atom located at the kink site. In order to visualize the movement of vacancies in the following discussion, it is important to keep in mind that the movement of the vacancy is the result of the movement of one of the atoms at its boundary and that the moving atom and the vacancy propagate in opposite directions. As in the preceding section we treat the annihilation of the vacancy and the migration of the vacancy on the flat terrace in two separate calculations.

We consider first the annihilation of the vacancy. The cluster utilized to describe this process is shown in Fig. 4(a). The shaded area represents a small part of an island containing a step with a kink. The nonshaded area represents a small fraction of the terrace of a (100) metal surface containing a vacancy. The migration path marked on the figure was found to exhibit the smallest activation energies and to provide the most probable mechanism for island decay. It illustrates a vacancy at the terrace site T moving first to the position S near the step from where it adsorbs the kink atom at K into the lower terrace. Other migration paths involving movement of the vacancy along the step are energetically unfavorable because the step atoms do not allow for sufficient space for the transition state of the vacancy to move upwards in a location near the step. Two-step processes in which the kink-atom first desorbs into the terrace as an adatom and later

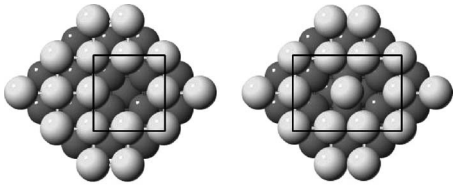

(a) (b)

FIG. 5. 51-atom clusters utilized to represent a vacancy of the (100) surface, moving from (a) its ground state to (b) the transition state.

recombines with the vacancy were also found to be energetically unfavorable. Finally, processes in which the kink-atom K and the terrace atom S move together away from the island exhibit even larger activation barriers because they involve both atoms moving simultaneously through the transition state.

Figures 4(b) and 4(c) show the variation of the energy and of the electric dipole along the migration path $T \leftarrow S \leftarrow K$, including intermediate positions. For each of the intermediate positions we varied the height of the adatom and we calculated the local equilibrium geometry. As in the case of the adatom, the energies at the transition bridge sites are larger than those of the ground state fourfold hollow sites, giving rise to an activation barrier for migration. The electrical dipoles are also larger at the transition states. In particular, the last $S \leftarrow K$ migration step in which the vacancy is annihilated, exhibits a large activation barrier, for here the kink-atom must jump over the step edge into a lower lying plane. In doing so, the kink atom must move through intermediate positions where it has fewer neighbors and are therefore energetically unfavorable. This means that vacancy migration leads to an island decay that is detachment limited. All three systems studied show qualitatively the same behavior as a function of migration distance, with Cu exhibiting somewhat larger energies and dipole moments because it has stronger atom-atom interactions. As in the preceding section we evaluate the formation energy of the vacancy as

$$E_v = E_v(T) - E_v(K), \tag{4}$$

where $E_v(T)$ and $E_v(K)$ are the energies at the locations T and K displayed in Fig. 4(b).

The clusters utilized to study the ground and the transition state of a vacancy in the terrace of the (100) surface are shown in Fig. 5. The reference cluster employed for the vacancy calculation has a different shape than that used in the adatom calculation, but it contains also 52 atoms and is also symmetrical in all three coordinates in order to minimize the error in the evaluation of the induced surface dipole. In the ground state shown in Fig. 5(a) one surface atom is missing and all the other ones are located above fourfold hollow sites of the underlying second layer. In the transition state shown in Fig. 5(b) one surface atom moves to the right and locates above a twofold bridge site of the second layer, and moves upwards by an amount Δz_v. Note that the vacancy moves to the left, i.e., in a direction opposite to that of the moving atom. The activation energy of the vacancy, ΔE_v, was calculated as the difference between the total energies of the cluster with the vacancy at the ground and transition states. The activation dipole $\Delta\mu_v$ was calculated in a similar fashion. Because of the symmetry of the cluster the electrical dipole of the vacancy, μ_v in its ground state, is just given by the electrical dipole of the cluster with the vacancy in the ground state [Fig. 5(a)]. These values are consistent with those deduced from Fig. 4(c) within about 8%.

TABLE II. Calculated values for the formation energy E_v, activation energy ΔE_v, surface dipole moment μ_v, activation dipole moment $\Delta\mu_v$, and change of height at the bridge site Δz_v for a vacancy at the Cu, Ag, and Au (100) surfaces. The transition state energy E_{v0}^{+}, given by the height of the first activation energy, and the transition state dipole μ_v^{+} are discussed in Sec. V.

	Cu	Ag	Au
E_v	0.56 eV	0.36 eV	0.42 eV
ΔE_v	0.78 eV	0.64 eV	0.72 eV
E_{v0}^{+}	1.52 eV	1.40 eV	1.31 eV
μ_v	0.076e Å	0.103e Å	0.055e Å
$\Delta\mu_v$	0.059e Å	0.055e Å	0.037e Å
μ_v^{+}	0.071e Å	0.123e Å	0.096e Å
Δz_v	0.15 Å	0.26 Å	0.31 Å

The numerical results for the vacancy calculation are summarized in Table II. Note that the activation energies and dipoles are smaller but of the same order of magnitude as those calculated for the adatom. Both for the adatom and for the vacancy the transition state involves the breaking of two bonds to the underlying second atom layer. However, in the case of the vacancy the severed bonds can interact with the surrounding atoms of the first atom layer leading to a reduction of the activation energy. Counting the number of broken bonds we also conclude that the formation energy of a vacancy should be of the same order of magnitude as the formation energy of an adatom, in qualitative agreement with our results. Using the GGA Boisvert and Lewis found a value of 0.42 eV for the activation barrier on the Cu(100) surface. As in the case of the adatom the activation barriers of these authors are smaller than the ones found in the present work.

We note that the surface dipole moment induced by the vacancy has the same sign as that produced by the adatom. The charge redistribution giving rise to the positive dipole moment of the vacancy is shown in Fig. 6, where we have plotted the charge density difference,

$$\Delta\rho_v = \rho(\mathrm{Au}_{51}) - \rho(\mathrm{Au}_{52}) + \rho(\mathrm{Au}), \tag{5}$$

for the Au surface. Here Au_{51} is the cluster displayed in Fig. 5(a) and Au_{52} the corresponding reference cluster without the vacancy. The last term in Eq. (5) represents the charge density of an isolated Au atom superposed at the location where the Au atom was removed in order to generate the vacancy, and is needed in order to compare systems with the same number of electrons. Since the charge density of an isolated atom is more compact than that of an atom in a solid, we see an accumulation of charge at the nucleus position. Aside

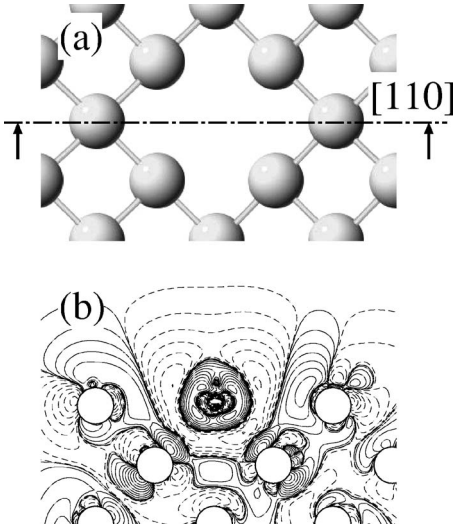

FIG. 6. (a) Schematic view of a vacancy at the an Au(100) surface in the ground state geometry. (b) Change in the charge density difference induced in the [110] plane by the creation of the vacancy. The continuous and dashed contour lines represent increase and decrease of charge, with densities given by $2n^3 \times 10^{-4}e$ Å^{-3}, for $n=-15,\ldots,15$.

from this somewhat artificial effect the charge density plot shows a depletion of charge on the volume of the vacancy. This charge depletion is the result of a charge transfer to the more densely packed and deeper lying atomic layers, which possess a larger local density of unoccupied states. This charge transfer is equivalent to a polarization of the atoms surrounding the vacancy, that redirects the bonds broken by the removal of one surface atom towards the atoms of the second layer.

IV. MIGRATION BY ATOM EXCHANGE

The clusters of Fig. 7 illustrate the exchange process for an adatom at the terrace of a (100) surface proposed by Feibelman to explain adatom migration in Al (100).[12] In this process one of the nearest neighbors of the adatom moves upward leading to a transition state in which the surface atom and the adatom form a metal dimer, as shown in Fig.

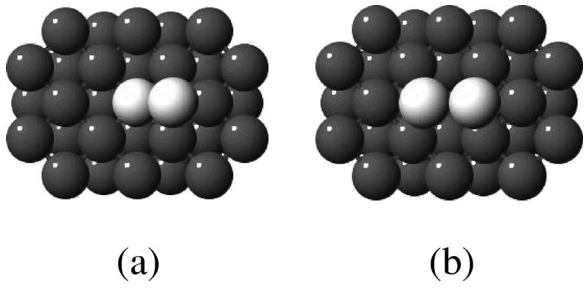

FIG. 7. (a) Cluster utilized to study the desorption of an atom from a kink in a step at the (100) surface by Feibelman's exchange process. Here D denotes the formation of the dimer. (b) Variation of the energy and (c) surface dipole moment along the migration path indicated in inset (a) for Au (full), Ag (dotted), and Cu (dashed).

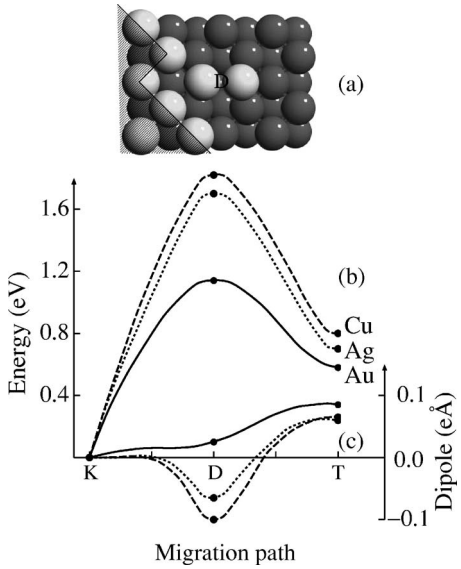

FIG. 8. 49-atom clusters utilized to represent migration by atom exchange at the (100) surface. (a) In the ground state we see an adatom in a fourfold hollow site. (b) In the transition state a neighbor of the adatom moves upwards leaving a vacancy in the surface plane and forms a dimer with the adatom. In a further stage (not shown) the adatom fills the vacancy.

7(b). In a further stage (not shown in the figure) the adatom fills the vacancy and the second atom is adsorbed at the surface one lattice spacing to the left. We calculated the ground state and transition state energies and dipole moments for the states shown in Figs. 7(a) and 7(b). For the transition state, we varied the interatomic distance and the height of the dimer above the surface.

Figure 8 describes the initial phase of the decay of an island by the exchange process assuming a kink in a surface step to be the initial state. The initial and final states of the exchange process are the same as in the case of adatom migration [cf. sites K and T in Fig. 1(a)]. Figure 8(a) illustrates the first transition state (denoted by D) along the migration path of the exchange process, which is characterized by a dimer adsorbed at the (100) terrace in a position near the step. One of the atoms of the dimer is the desorbed kink atom, the other one an atom from the first atom layer of the terrace, that moved higher. Figure 8(b) displays the energy variation along migration path for the exchange process. We observe a rather large activation barrier for the Cu and Ag surfaces, such that for these systems the exchange process is not likely to provide an energetically favorable mechanism for mass transport. On the other hand, for the Au surface the activation barrier is of the same order of magnitude as that found for the adatom so that the exchange process is expected to be energetically accessible for this system. Pseudopotential calculations predict exchange diffusion for the Au(100) surface.[25] The smaller activation energy for the Au dimer appear to be a result of the relativistic contraction of the Au core density.

Table III summarizes our main results for the exchange process. We note that for the Cu, Ag, and Au surfaces the activation energies of the exchange process are larger than

TABLE III. Calculated values for the formation energy E_d, activation energy ΔE_d, and surface dipole moment μ_d of a dimer at the Cu, Ag, and Au (100) surfaces. The transition state energy E_{v0}^{+} given by the height of the first activation energy, and the transition state surface dipole moment μ_d^{+} are discussed in Sec. V.

	Cu	Ag	Au
E_d	0.80 eV	0.70 eV	0.58 eV
ΔE_d	1.02 eV	1.00 eV	0.60 eV
E_{d0}^{+}	1.82 eV	1.70 eV	1.14 eV
μ_d	0.067e Å	0.070e Å	0.114e Å
μ_d^{+}	−0.099e Å	−0.065e Å	0.026e Å

that for the Al surface.[12] The reason for these larger energies is that for transition metals with only s and d orbitals it is not possible to produce strong directional bonds needed to bind the dimer. The calculated distance between the two atoms of the dimer was found to be only slightly smaller (of the order of 0.1 Å) than the bulk interatomic spacing.

For the Cu and Ag surfaces the electric dipole moment of the dimer turned out to be negative, while for the Au surface we found a dipole moment which is positive but much smaller than that of the adatom. In Fig. 9 we show the redistribution of the charge density due to the interaction of the dimer with the Au(100) surface, calculated as

$$\Delta\rho_d = \rho(\mathrm{Au}_{49}) - \rho(\mathrm{Au}_{47}) - \rho(\mathrm{Au}_2), \tag{6}$$

where Au_{52} is the cluster displayed in Fig. 7(b), and Au_{49} the corresponding reference cluster without the dimer. Here $\rho(Au_2)$ is the charge density of a Au dimer with an interatomic distance equal to the optimized value from the surface calculation. Observe the increased charge density between the two Au atoms of the dimer leading to a reduction of the surface dipole moment.

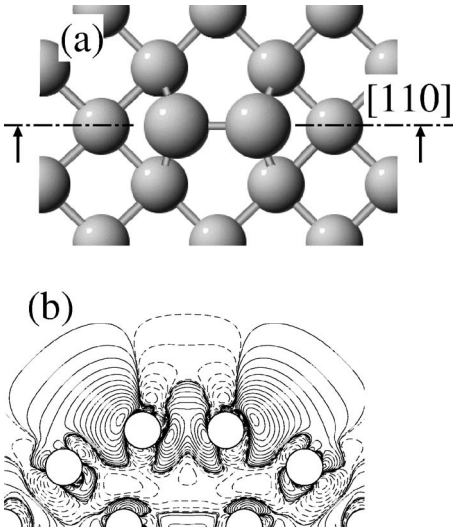

FIG. 9. (a) Schematic view of an atom dimer in an exchange process at the Au(100) surface. (b) Change in the charge density difference induced in the [110] plane by the formation of the dimer. The continuous and dashed contour lines represent increase and decrease of charge, with densities given by $2n^3 \times 10^{-4} e\ Å^{-3}$, for $n = -15, \ldots, 15$.

An interesting conclusion of this calculation is that the resulting dipole for the Cu and Ag dimers is opposite than that expected according to the Smoluchowsky principle.[26] The Smoluchowsky principle is successfully used in theoretical models with sharp potentials to predict the formation of surface dipoles. However, in general the charge distribution is not determined by the minimization of the kinetic energy but rather by minimization of the total energy which is mainly controlled by the potential energy. The kinetic energy follows the potential energy according to the Virial theorem. This means that the atomic charge densities polarize in a direction determined by the underlying potential.

V. ENERGY OF POINT DEFECTS ON INTERFACES HELD AT A CONSTANT POTENTIAL

In this section we present a brief discussion of how the electric dipole influences the phenomenon of island decay through formation and diffusion of point defects at solid-electrolyte interfaces. For a detailed treatment of this subject see Ref. 11.

In the preceding sections we see that the formation of point defects gives rise to the development of an electrical dipole moment localized at the surface. This electrical dipole produces a change in the work function of the surface given by

$$\Delta\phi = \rho\mu_{pd}/\epsilon_0, \tag{7}$$

where μ_{pd} is the dipole of the point defect, ρ is the density of point defects, and ϵ_0 is the vacuum permittivity. Both the electric dipole moments and the work function changes depend on the actual positions of the point defects on the surface. However, to the purpose of this discussion we may assume that all the point defects adsorb at equivalent surface sites, for at the end of the argument we will only be interested in the limiting case $\rho \to 0$.

If the solid surface is kept at a constant potential ϕ by an external source, the formation and diffusion of point defects will give rise to a flow of charge from the battery to the surface in order to compensate for the work function changes induced by the point defect dipoles. To first order in the defect density ρ the charge density on the surface with defects can be written as

$$\sigma_{pd}(\phi) = \sigma_0(\phi + \Delta\phi) = \sigma_0(\phi) + \frac{\partial\sigma_0}{\partial\phi}\Delta\phi, \tag{8}$$

where σ_0 is the charge density of the surface without defects and $\Delta\phi$ is given by Eq. (7). In this expression σ_{pd} and $\Delta\phi$ are dependent of the local position of the point defect along the surface.

The flow of charge to the surface responsible for keeping the surface potential at the constant value ϕ, requires a certain amount of work, that must be provided by the battery. With the aid of Eqs. (7) and (8) the external work per point defect can be calculated as

$$\Delta E(\phi) = -\lim_{\rho\to 0}\frac{1}{\rho}\int_{\phi_{pzc,0}}^{\phi}[\sigma_{pd}(\phi') - \sigma_0(\phi')]d\phi' \tag{9}$$

$$= -\frac{\mu_{pd}}{\epsilon_0}\sigma_0(\phi), \tag{10}$$

where $\phi_{pzc,0}$ is the potential of zero charge of the surface without defects, defined by

$$\sigma_0(\phi_{pzc,0}) = 0. \tag{11}$$

The energy $\Delta E(\phi)$ provided by the battery amounts to an additional potential-dependent energy contribution involved in the formation and diffusion of a single point defect. Note that an intrinsically microscopic or local definition of $\Delta E(\phi)$ is not possible for this energy is provided by an external macroscopic source. For the ideally polarizable electrolyte interface with a clean solid surface we may interpret Eq. (10) as the energy of the point charge dipole moment in an electric field $\mathcal{E}=\sigma/\epsilon_0$ localized at the interface. However, in a real interface containing specifically adsorbed ions this interpretation would be misleading. These ions are normally provided by the electrolyte and their concentration is in general a function of the surface potential. They lead to a charge density on the surface that may be quite inhomogeneous. In the presence of specific adsorption $\mathcal{E}$ represents an average electric field that includes the contribution of the adsorbed ions and is not necessarily equal to the field acting on the electrical dipole of the point defect. This means that the energy for creating and migrating a point defect on a charged surface depends on the concentration and potential dependence of the specific adsorption on the surface.

It may be worth pointing out that $\sigma_0(\phi)$ in Eq. (10), which is responsible for the potential dependence of the total activation energy diffusion of the point defect, is actually the experimentally measured surface charge density. With the aid of Eq. (11) and as long as the system remains in the linear regime we may safely write this surface charge density as

$$\sigma_0(\phi) = C_0(\phi - \phi_{pzc}), \tag{12}$$

where C_0 is the capacitance of the surface without defects at the potential of zero charge. Note that C_0 includes the charging effects due to specific adsorption.

The rate of surface transport is determined by the highest value of the total energy along migration path of the point defect, E^+, defined with reference to an initial state consisting of a straight step with a kink.[27] With the aid of Eqs. (10) and (12) this energy can be written as

$$E^+ = E_0^+ - \frac{\mu_{pd}^+}{\epsilon_0}C_0(\phi - \phi_{pzc}), \tag{13}$$

where μ_{pd}^+ is the electric dipole moment and E_0^+ the total formation energy of the point defect for the uncharged surface, both evaluated at the location with largest activation barrier. These quantities are determined by the local electronic interaction between the point defect and the surface. While the considerations above hold for a surface in any environment (including vacuum), they become relevant only for surfaces in contact with an electrolyte, where the charge densities can take very large values (of about 0.1 to 0.4 e/atom). Using a value for the surface capacitance $C_0 \approx 50\ \mu\mathrm{F/cm^2}$, typical for metal-electrolyte interfaces used in electrochemistry, we may estimate

$$E^+ \approx E_0^+ - 5.6\left(\frac{\mu_{pd}^+}{e\text{Å}}\right)\left(\frac{\phi - \phi_{pzc}}{\mathrm{V}}\right)\ \mathrm{eV}. \tag{14}$$

The electronic part of the transition state energy E_0^+ in Eq. (14), involves the energies of three different processes: (1) the formation of the point defect by desorption of a kink atom E_{pd}, (2) the overcoming of the first activation barrier E_{fab}, and (3) the diffusion of the point defect away from (to) the island ΔE_{pd}. For adatoms, the first activation barrier is smaller than the subsequent ones, such that $E_0^+ = E_{pd} + \Delta E_{pd}$ (see Table I). This means that adatom mediated island decay is diffusion limited. By contrast for vacancies and dimers the highest activation energies occurs at the first migration barrier, leading to detachment-limited decay characterized by $E_0^+ = E_{fab}$ (see Tables II and III). In the preceding sections we found that for both adatoms and vacancies the variation of the surface dipole moment along the migration path correlates with that of the local electronic energy of the point defect, in such a way that for positive potentials the electrostatic energy tends to quench the activation barriers, and to increase the mobility of the point defects. Using Eq. (14) we conclude that for typical ranges of potentials used in electrochemistry the electrostatic renormalization of the point-defect energy is smaller in magnitude than the electronic effects. This means that the positions of the transition states for point-defect migration is determined by the local maxima of the electronic interaction of the point defect with the surface, located at bridge sites of the surface.

It can be shown that for island decay both the electronic energy E_0^+ and the potential dependent dipole energy $\Delta E(\phi)$ combine in a single thermodynamic process characterized by the transition state energy E^+.[27] Therefore, the probability of creating and propagating a point defect on a metal surface as a function of the surface potential is proportional to

$$\exp[C_0\mu^+(\phi - \phi_{pzc})]. \tag{15}$$

This expression leads to an exponential dependence in the decay rate of islands as function of the surface potential. Our numerical results imply that for positively charged surfaces island decay is enhanced by adatom diffusion-limited processes (a phenomenon customarily known as electrochemical annealing) and for the negatively charged surfaces mass transport is slowed down by the potential in all three systems studied in this work. As mentioned in Sec. IV the exchange process is only likely to play a role for neutral Au surfaces.

The conclusions presented in this section have been applied in Ref. 11 to formulate a quantitative description of the two-dimensional Oswald-ripening on Au (100) surfaces.

VI. SUMMARY AND CONCLUSIONS

We have applied the LDA and the cluster method to study the phenomenon of island decay by surface diffusion by adatoms, vacancies and dimers, both at a kink-site in a straight

step and at the terrace of the (100) surfaces of Cu, Ag, and Au. We stressed the importance of using the kink atom as the initial condition for the thermodynamic description of island decay and we implemented this condition in our calculations by numerically simulating the removal of an atom at a kink site. Although in the present work we explicitly considered only the process of island decay, our arguments are also valid for island growth, since both processes are thermodynamically equivalent.

The central result of this work is that both the adatoms and the vacancies exhibit a positive dipole moment, i.e., an electrical dipole with the positive end pointing away from the metal surface. We showed that this is due to the charge of the adatom (or that of the atoms surrounding the vacancy) polarizing towards the metal where there are more atoms and the density of unoccupied states is larger. The general nature of this phenomenon lead us to expect that the positive dipole moment is a property of adatoms and vacancies on all metal surfaces. The Au dimer also exhibits a small positive dipole moment. However, for the Cu and Ag dimers we found that a stronger bond between the two atoms of the dimer leads to negative values for the dipole moment.

We show that all activation and formation energies of point defects exhibit a linear dependence on the surface potential. This means that the application of a positive potential to the surface leads to an exponential increases of the mobility of adatoms and vacancies on the surface, and that for negative surface potentials the diffusion of adatoms and vacancies is inhibited. We also see that the exchange process has no relevance for the Cu and Ag surfaces but is expected to contribute to the surface dynamics of neutral Au surfaces.

We corroborated the well-known results that vacancies exhibit their largest activation barrier at the annihilation process, which leads to detachment-limited decay, and that for adatoms the first activation barrier is small, leading to diffusion-limited decay. We also found that while adatoms tend to stick to steps and to move freely along them, the motion of vacancies along the steps is blocked. This means that steps are likely to contain a large density of isolated adsorbed atoms that may readily desorb onto the terrace. On the other hand, vacancies can only interact with the kink site, which greatly reduces the cross section of the vacancy-island interaction. These considerations do not affect the equilibrium concentration of point defects on terraces but may be important in the context of dynamical simulations of surface transport.

As we stated in the introduction, our reported energies are likely to be an overestimation of the actual physical values. We wish also to remark that although we considered a large number of migration paths for the different point defects, we do not claim our study to be exhaustive. We are also aware that the present study leaves many unanswered questions. In particular, our results appear to be in contradiction with the interpretation of experimental results for Cu(100) presented by Klünker *et al.*, that concludes that the surface decay takes place by detachment-limited vacancy migration.[28] These authors found that for the Cu(100) surface the total activation energy amounts to $E_0^+=0.8$ eV, while our value is ~ 1.5 eV for both vacancies and adatoms. This discrepancy between theory and experiment is certainly larger than that expected as a result of the inaccuracies of the LDA and suggests that there may exist additional reaction paths, which we may have failed to consider. It is also possible that the surface relaxation produced by a vacancy is more extended than the one we allowed for in this work. In spite of these limitations in the scope of our work, we wish to point out that most of our conclusions are based on physical results of qualitative nature which are expected to be independent of any approximations employed in the calculations.

ACKNOWLEDGMENTS

The authors gratefully acknowledge illuminating discussions with M. Giesen, G. Beltramo, and W. Schmickler, and appreciate the financial support provided to one of the authors (H.I.) by the Fond der Chemischen Industrie.

[1] M. S. Zei and G. Ertl, Surf. Sci. **442**, 19 (1999).
[2] J. M. Doña and J. González Velasco, Surf. Sci. **274**, 205 (1992).
[3] M. Hidalgo, M. L. Marcos, and J. González Velasco, Appl. Phys. Lett. **67**, 1486 (1995).
[4] J. J. Martínez Jubrías, M. Hidalgo, M. L. Marcos, and J. González Velasco, Surf. Sci. **366**, 239 (1996).
[5] N. Hirai, H. Tanaka, and S. Hara, Appl. Surf. Sci. **130-132**, 506 (1998).
[6] N. Hirai, K. I. Watanabe, and S. Hara, Surf. Sci. **493**, 568 (2001).
[7] K. Kubo, N. Hirai, T. Tanaka, and S. Hara, Surf. Sci. **565**, L271 (2001).
[8] M. Giesen, M. Dietterle, D. Stapel, H. Ibach, and D. M. Kolb, Surf. Sci. **384**, 168 (1997).
[9] M. Giesen, R. Randler, S. Baier, H. Ibach, and D. M. Kolb, Electrochim. Acta **45**, 527 (1999).
[10] M. Giesen and D. M. Kolb, Surf. Sci. **468**, 149 (2000).
[11] M. Giesen, G. Beltramo, S. Dieluweit, J. E. Müller, H. Ibach, and W. Schmickler, Surf. Sci. **595**, 127 (2005).
[12] P. J. Feibelman, Phys. Rev. Lett. **65**, 729 (1990).
[13] R. Stumpf and M. Scheffler, Phys. Rev. B **53**, 4958 (1996).
[14] B. D. Yu and M. Scheffler, Phys. Rev. Lett. **77**, 1095 (1996).
[15] H. M. Polatoglou, M. Methfessel, and M. Scheffler, Phys. Rev. B **48**, 1877 (1993).
[16] G. Boisvert, L. J. Lewis, M. J. Puska, and R. M. Nieminen, Phys. Rev. B **52**, 9078 (1995).
[17] G. Boisvert, L. J. Lewis, and M. Scheffler, Phys. Rev. B **57**, 1881 (1998).
[18] G. Boisvert and L. J. Lewis, Phys. Rev. B **56**, 7643 (1997).
[19] C. Lee, G. T. Barkema, M. Breeman, A. Pasquarello, and R. Car, Surf. Sci. **306**, L575 (1994).
[20] J. E. Müller, R. O. Jones, and J. Harris, J. Chem. Phys. **79**, 1874 (1983).
[21] S. Walter, V. Blum, L. Hammer, S. Müller, K. Heinz, and M. Giesen, Prog. Surf. Sci. **498**, 155 (2000).

[22] H. Li, J. Quinn, Y. S. Li, D. Tian, F. Jona, and P. M. Marcus, Phys. Rev. B **43**, 7305 (1991).
[23] V. Blum, Ch. Rath, S. Müller, L. Hammer, K. Heinz, J. M. García, J. E. Ortega, J. E. Prieto, O. S. Hernán, J. M. Gallego, A. L. Vazquez de Parga, and R. Miranda, Phys. Rev. B **59**, 15966 (1999).
[24] J. E. Müller, Surf. Sci. **178**, 589 (1986).
[25] B. D. Yu and M. Scheffler, Phys. Rev. B **56**, R15569 (1997).
[26] R. Smoluchowski, Phys. Rev. **60**, 661 (1941).
[27] M. Giesen, Prog. Surf. Sci. **68**, 1 (2001).
[28] C. Klünker, J. B. Hannon, M. Giesen, H. Ibach, G. Boisvert, and L. J. Lewis, Phys. Rev. B **58**, R7556 (1998).